Star Polymers in Solvents of Varying Quality

Sebastian Huissmann,* Ronald Blaak, and Christos N. Likos

Institut für Theoretische Physik II: Weiche Materie, Heinrich-Heine-Universität Düsseldorf, Universitätsstraβe 1, D-40225 Düsseldorf, Germany

Received October 16, 2008; Revised Manuscript Received February 3, 2009

ABSTRACT: We perform molecular dynamics simulations on star polymers with different functionalities in solvents of various quality. The radial distribution of the monomers around the star center follows the predictions stemming from scaling theory. We demonstrate that not only the scaling but also the diffuse regime of the chains far from the center can be described by universal functions predicted from theory. Moreover, we measure the effective force between two such stars and show that it is purely repulsive for athermal solvents, with the repulsion being reduced for worsening solvent quality and an attraction appearing at intermediate star distances close to Θ-solvent conditions. A mean-field-type analytical approach is set forward to calculate the effective potential between star polymers not too close to the estimated Θ point.

I. Introduction

Star-shaped polymers[1] are a very important class of branched macromolecules. Because of their particular architecture, which consists of f arms attached to a common center, they serve as soft colloids that bridge the gap between hard spheres and polymer chains.[2,3] Star polymers also serve as excellent systems for describing the shapes and phase behavior of block copolymer micelles, for which recent experiments have established the occurrence of liquid-fcc-bcc transitions,[4,5] which is in agreement with theoretical predictions for star polymers.[3] Because the functionality, f, serves as a means to control the softness and penetrability of the stars, their rheological properties are quite distinct from those of hard spheres.[6,7] Indeed, the vitrification behavior of athermal star polymers, although it can be cast in the language of crowding and caging, as is the case with hard spheres,[8] also hides a host of surprises when mixtures of stars with homopolymer chains[9] or with smaller star polymers are considered.[10,11] Here melting and re-entrant vitrification to a variety of novel arrested states has been found by a combination of experimental and theoretical efforts.

Apart from the functionality, f, there also exist other ways to tune the conformations of star polymers and the ensuing softness of the effective interactions[12,13] between the same. One possibility is offered by charging a fraction of the monomers along the backbone of the arms,[14−16] allowing control via the pH and the salinity of the solution. Within the realm of neutral stars, one can affect the quality of the solvent by changing the temperature, T; typically, the quality of organic solvents worsens with decreasing T; the opposite is true for aqueous solvents. The vast majority of investigations on star polymers to date has focused on the case of athermal solvents, which can be modeled by a purely repulsive monomer−monomer interaction. Much less is known about solvents of worsening quality, which are modeled by additional long-range attractions between the monomers induced by unbalanced van der Waals forces. The standard analytical model describing the conformations of stars dependent on solvent quality, f, and arm degree of polymerization, N, is attributable to Daoud and Cotton[17] and is known as the 'blob model'; we will return to it in detail below.

The Θ point for a given system is defined as the Boyle point, that is, the point at which the second virial coefficient between two such particular molecules becomes zero. However, for a fixed Hamiltonian, for example, fixed bonded and nonbonded monomer−monomer interactions in a star polymer, it will depend on N as well as on the functionality. Only in the limit $N \rightarrow \infty$ does the Boyle point becomes independent of the topology. Irrespective of the precise location of the Θ point for a given star polymer, the fact remains that when solvent quality worsens, the effective attraction between the monomers increases. The associated changes in the form and effective interactions between thermal stars are of high current interest because of the possibilities that open up in steering macroscopic properties via temperature changes.

Although a number of simulation studies have been devoted to star polymers in good or athermal solvents,[18−23] simulations of star polymers in thermal solvents are more scarce. A very important work, published 20 years ago, was carried out by Batoulis and Kremer.[24] They performed extensive on-lattice simulations of stars with up to $f = 12$ arms to determine the location of the Θ temperature for stars and its relation to that of individual chains. It was established that the Θ condition for stars is fulfilled at a lower temperature than that for chains, and it approached the latter from below as $N \rightarrow \infty$. Bishop and Clarke[25] employed Brownian dynamics simulations to examine the scaling of the radius of gyration, R_G, with the degree of polymerization, N, dependent on the solvent quality. They found $R_G^2 \propto N^{6/5}$ for athermal solvents, $R_G^2 \propto N$ for Θ solvents, and $R_G^2 \propto N^{2/3}$ for the fully collapsed state, which is in full agreement with the Flory exponent, $\nu_F = 3/5$, the random-walk exponent, $\nu_0 = 1/2$, and the compact-sphere exponent, $\nu_c = 1/3$, respectively. Grest[26] performed later extensive, off-lattice simulations of stars with $3 \leq f \leq 80$ arms, in which he examined the conformations (density profiles) and distributions of the center-to-end radius, R, of the same. By varying the solvent quality, the transition of the scaling behavior[17] of $\rho(r)$ from $\rho(r) \propto r^{-4/3}$ (athermal solvents) to $\rho(r) \propto r^{-1}$ (Θ solvents), where r is the distance from the star center that lies within the corona radius, was confirmed.

All preceding studies have been concerned with isolated stars, aiming at a description of either the Θ temperature itself or the size and density profiles in the scaling region, in which $\rho(r)$ is a power law of r. However, a number of important issues are still open. First, it is desirable to have a quantitative description of $\rho(r)$ for the whole r range, including the diffuse polymer layer for $r \gg R$, in a fashion similar to that of athermal stars.[23,27] More importantly, the interactions and correlations between star polymers in solvents of varying quality have hardly received any attention, at least not by means of a microscopic approach. Benhamou et al.[28,29] have employed field-theoretical methods

* Corresponding author. E-mail: sebastian@thphy.uni-duesseldorf.de.

10.1021/ma8023359 CCC: $40.75
Published on Web 03/12/2009

to determine the effective center-to-center force $F(r)$ between two stars exactly at the Θ point. They found a functional form $F(r) = k_B T A_{f_1 f_2}[r \ln(R^2/r^2)]^{-1}$ for $r \ll R$, where k_B is the Boltzmann constant and $A_{f_1 f_2} = f_1 f_2 (f_1 + f_2 - 2)/22$ is a prefactor that depends on the functionalities of the two interacting stars, which are generally different from each other. Although this form is exact, its validity in both the temperature domain and its range is limited to $T = T_\Theta$ and $r \ll R$, respectively.

The issue of interactions between thermal, deformable colloids has become of high topical interest lately because a number of experimental studies have been performed with the goal of exploring the question of tuning the phase behavior and the rheology of soft particles, such as thermosensitive microgels[30−33] or, precisely, star polymers. An impressive manifestation of the sensitivity of stars to temperature changes is offered by the phenomenon of thermally reversible gelation in a concentrated solution of the same.[34,35] Here a concentrated system is arrested under athermal conditions because the stars are swollen, leading to crowding.[8] However, upon lowering of the temperature, the stars shrink, and the system liquefies and flows. The shrinking of the stars is indeed one factor that enters the game of rheology modification but certainly not the only one. The star−star interactions themselves are most certainly affected by the solvent quality. Likos et al.[36] have employed an effective interaction between stars in the neighborhood of the Θ point, which leads to a very good description of SANS data; however, this interaction is based on self-consistent-field considerations;[37−39] that is, it is not of microscopic origin. Furthermore, the effective potential of Likos et al.,[36] although it features weaker repulsions than its counterpart for athermal solvents,[2] remains repulsive at all separations and offers no way of determining at which temperature the attractions between the stars set in. In recent publications, Rissanou et al.[40−42] employed the effective interaction of ref 36 to rationalize the experimental findings of reversible gelation[34,35] with remarkable success. The key ingredient employed was the shrinking of the star upon temperature changes, which implies that the functional form of the interaction remains invariant when distances are scaled on the star size. Despite the success of these approaches, the current state is unsatisfactory because a precise knowledge of the temperature-dependent form of the interaction is important to understand fully not only reversible gelation per se but also other phenomena, such as the adsorption of stars on surfaces[43] or the dynamics of the solution and issues of convexity of the dynamical, intermediate scattering function,[44−49] $\phi(q, t)$, at fixed wavenumber, q, as a function of time, t.

The purpose of this article is to address the open questions mentioned above. To this end, we introduce a new microscopic modeling of monomer−monomer interactions at solvents of arbitrary quality that is free of the usual truncation problems of the Lennard-Jones interaction and analyze conformations and interactions for solvents of varying quality by means of molecular dynamics (MD) simulations and theoretical modeling. We find that the star−star interactions remain repulsive down to temperatures above the stars' Θ temperature, with attractions developing as one approaches it. The rest of the article is organized as follows: In Section II, we present our simulation model and the quantities measured. In Section III, we show the results regarding the estimation of the Θ temperature for stars, the coil-to-globule transition, and the density profiles, including their theoretical modeling. In Section IV, we turn our attention to the effective interaction between thermal star polymers and compare the results of the simulation with those of a theoretical, perturbation approach that we introduce. Finally, in Section V, we summarize and draw our conclusions.

II. Simulation Model

According to the widely used scaling approach for polymeric systems, the structure of star polymers on large length scales is mainly determined by statistics and is independent of the specific chemical nature of the polymer, at least in the limit $N \gg 1$. It is therefore possible to obtain the correct mesoscopic properties from a simple microscopic model where only the relevant molecular characteristics are incorporated. The excluded volume effects for real polymers as well as the solvent-mediated interactions induce long-range correlations between segments along the chain that need to be considered in the model. Here we employ the standard star polymer model proposed by Grest et al.,[18] which was later extended by Jusufi et al.[21] to the case of two stars, and modify it to include solvent effects to obtain the effective interaction in thermal solvents. Although the focus of this work is on thermal stars, we will also always show the results obtained for the athermal case for the purpose of both reproducing the known facts as a confirmation and providing a comparison with thermal solvents.

A. Athermal Solvents. We employ a monomer-resolved bead-spring model in the continuum. In this case, the effective monomer−monomer interactions are purely repulsive because the combined effect of the bare monomer−monomer, monomer−solvent, and solvent−solvent interactions is to cancel the dispersion forces between monomers that operate in the absence of solvent. The steric interactions between any pair of monomers at a relative distance, r, are modeled via the purely repulsive, truncated and shifted Lennard-Jones potential,[50] $v_0(r)$

$$v_0(r) = \begin{cases} 4\epsilon\left[\left(\frac{\sigma_{LJ}}{r}\right)^{12} - \left(\frac{\sigma_{LJ}}{r}\right)^{6} + \frac{1}{4}\right] & r \le 2^{1/6}\sigma_{LJ} \\ 0 & r > 2^{1/6}\sigma_{LJ} \end{cases} \quad (1)$$

where the interaction strength, ϵ, will be the unit of energy and the monomer diameter, σ_{LJ}, will be the unit of length. The monomers constituting a chain are held together by connecting sequential monomers with inelastic springs whose interaction is described by the so-called finite extensible nonlinear elastic (FENE) potential $v_{ch}(r)$

$$v_{ch}(r) = \begin{cases} -\frac{1}{2}k_{FENE}\left(\frac{R_0}{\sigma_{LJ}}\right)^2 \ln\left[1 - \left(\frac{r}{R_0}\right)^2\right] & r \le R_0 \\ \infty & r > R_0 \end{cases} \quad (2)$$

In our simulations, we set the maximum elongation length to $R_0 = 1.5\sigma_{LJ}$ and the spring constant to $k_{FENE} = 30\epsilon$. The f polymer chains (functionality of the star) are connected to a central core particle whose radius, R_c, is large enough to avoid overlaps of the innermost monomers. Its larger size with respect to the monomers requires a slightly modified interaction, which is achieved by shifting the monomer repulsions and bonds over the core radius and adding a central hard core repulsion. This results in a monomer-core repulsion $v_0^c(r)$ and bonding interaction $v_{ch}^c(r)$

$$v_0^c(r) = \begin{cases} \infty & r \le R_c \\ v_0(r - R_c) & r > R_c \end{cases} \quad (3)$$

$$v_{ch}^c(r) = \begin{cases} \infty & r \le R_c \\ v_{ch}(r - R_c) & r > R_c \end{cases} \quad (4)$$

where the latter interaction is restricted to the first monomer in each polymer chain only. The size of the core particle follows from assuming an even area distribution for the innermost monomers and hence depends explicitly on the functionality of the polymer by

$$R_c = \frac{1}{4}\sigma_{LJ}\sqrt{f} \tag{5}$$

In the MD simulations performed on this model, we implemented the velocity Verlet algorithm[51] to integrate the equations of motion and fixed the temperature at $T_0 = 1.2\epsilon/k_B$ using a Berendsen thermostat.[52] Time is measured in units of $\tau = (m\sigma_{LJ}^2/\epsilon)^{1/2}$, and up to 10^6-10^7 time steps of $\delta t = 0.003\tau$ have been used for the simulations, with an appropriate fraction of them for the equilibration of the system.

The quantities measured are presented below. The radius of gyration, R_G, as well as the monomer density profile, $\rho(r)$, around the star center are the two measures of the extension and the profile of single stars. The former is defined as

$$R_G^2 = \frac{1}{2(Nf)^2}\left\langle \sum_{i=1}^{Nf}\sum_{j=1}^{Nf}(\mathbf{r}_i - \mathbf{r}_j)^2 \right\rangle \tag{6}$$

where $\mathbf{r}_i$ is the coordinate of the ith monomer and $\langle ... \rangle$ denotes the statistical average. The latter is given by the relation

$$\rho(r) = \left\langle \sum_{i=1}^{Nf} \delta(\tilde{\mathbf{r}}_i - \mathbf{r}) \right\rangle \tag{7}$$

where $\tilde{\mathbf{r}}_i$ is the coordinate of the ith monomer and $\mathbf{r}$ is an arbitrary point in space, both measured in a coordinate system with the origin at the star center; finally, $r \equiv |\mathbf{r}|$.

The effective force, $\mathbf{F}_i$, acting on the center of the ith star is a quantity that can be measured in a simulation involving two stars; evidently, $\mathbf{F}_1 = -\mathbf{F}_2$. By fixing the core particles of two star polymers at positions $\mathbf{R}_1$ and $\mathbf{R}_2$, we can measure their effective interstar force as function of their relative distance, $D = |\mathbf{R}_2 - \mathbf{R}_1|$. If we denote the position of the lth monomer in the kth arm of star polymer, i, by $\mathbf{r}_{kl}^{(i)}$, then we can write the average force, $\mathbf{F}_i$, on the center of star i as a canonical average over all LJ interaction of the monomers of both stars and the FENE interaction of the innermost monomers with only the central core

$$\mathbf{F}_i(D) = \left\langle -\nabla_{\mathbf{R}_i}\left[\sum_{j=1}^{2}\sum_{k=1}^{f}\sum_{l=1}^{N} v_0^c(|\mathbf{r}_{kl}^{(j)} - \mathbf{R}_i|) + \sum_{k=1}^{f} v_{ch}^c(|\mathbf{r}_{k1}^{(i)} - \mathbf{R}_i|)\right]\right\rangle \tag{8}$$

B. Thermal Solvents. By choosing an adequate combination of monomers and solvent, it is possible to make the effective interaction between polymer segments attractive;[53] this corresponds to a worsening of the solvent quality. In this case of dominant van der Waals interactions, the system can minimize its energy by minimizing the interface between monomer and solvent particles. This results in an effective attraction between monomers, provided that the temperature is small enough. When the thermal energy is larger than the decrease in energy for two monomers approaching each other, this attraction can be neglected and good solvent conditions are obtained. In simulations without explicit solvent, such as the ones we perform here, this effect is usually modeled by a modification of the monomer−monomer interaction of eq 1, which reads[26,54]

$$v_{mm}(r) = \begin{cases} 4\epsilon\left[\left(\frac{\sigma_{LJ}}{r}\right)^{12} - \left(\frac{\sigma_{LJ}}{r}\right)^{6} - \left(\frac{\sigma_{LJ}}{r_c}\right)^{12} + \left(\frac{\sigma_{LJ}}{r_c}\right)^{6}\right] & r \le r_c \\ 0 & r > r_c \end{cases} \tag{9}$$

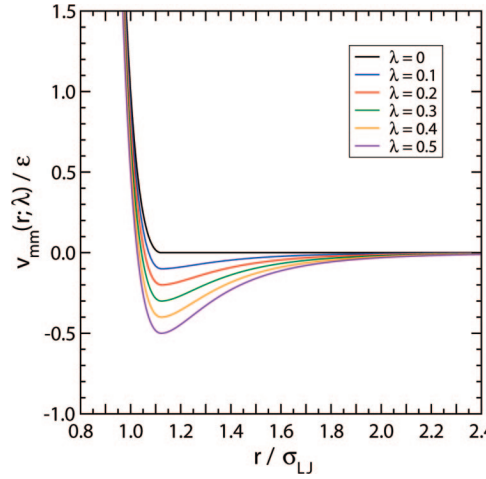

Figure 1. Effective monomer−monomer interaction, eq 10, for different solvent qualities, as modeled by the parameter λ.

where r_c is varied to tune the attractions. The choice $r_c = 2^{1/6}\sigma_{LJ}$ yields the athermal conditions of eq 1, whereas $r_c > 2^{1/6}\sigma_{LJ}$ models worsening solvent quality, with the attractions becoming stronger as r_c grows.

A slight drawback of the modeling via eq 9 above is that the force $f_{mm}(r) = -dv_{mm}(r)/dr$ is discontinuous at r_c for $r_c > 2^{1/6}\sigma_{LJ}$. To avoid this problem, we proceed here with a different modeling of the attraction strength by introducing the interaction parameter λ, which plays the role of an inverse temperature and modifies the bare monomer−monomer interaction, $v_0(r)$, by adding an attractive contribution to it as follows

$$v_{mm}(r;\lambda) = v_0(r) + \lambda v_{att}(r) \tag{10}$$

where the effective attraction potential, $v_{att}(r)$, is given by

$$v_{att}(r) = \begin{cases} -\epsilon & r \le 2^{1/6}\sigma_{LJ} \\ 4\epsilon\left[\left(\frac{\sigma_{LJ}}{r}\right)^{12} - \left(\frac{\sigma_{LJ}}{r}\right)^{6}\right] & r > 2^{1/6}\sigma_{LJ} \end{cases} \tag{11}$$

Apart from fixing the force discontinuity problem, this approach also has certain advantages for the theoretical description of the effective star−star force (Section IV), because it allows us to set up a perturbation theory approach to this quantity using λ as an expansion parameter. Our approach is similar to the one employed by Steinhauser[55] in his study of polymer chains in thermal solvents, albeit with a different modeling of the attractive part, $v_{att}(r)$. The expectation values of the quantities of interest presented in Section II.A, eqs 6−8, were calculated in the same way as those for thermal solvents, with the formal substitution $v_0(r) \rightarrow v_{mm}(r;\lambda)$. Clearly, $\lambda = 0$ brings us back to the athermal limit, whereas the solvent quality effectively worsens as λ grows; the original, full Lennard-Jones interaction is obtained for $\lambda = 1$. In Figure 1, the segment−segment interaction potential is shown for different solvents.

III. Single Stars

A. Coil-to-Globule Transition. To investigate the coil-to-globule transition and to estimate the location of the Θ temperatures for the stars, we have performed simulations of our star polymer model, restricting ourselves to stars with functionalities $f = 10$, 18, and 30 and a polymerization per $N = 50$. The shape and size of polymers strongly depend on temperature and the chemical composition of the system under consideration. They range from a swollen coil for the athermal solvent to a compact globule for a poor solvent, as is illustrated in Figure 2. Following the direction of the arrows there, we see that for $\lambda = 0$, the athermal case,

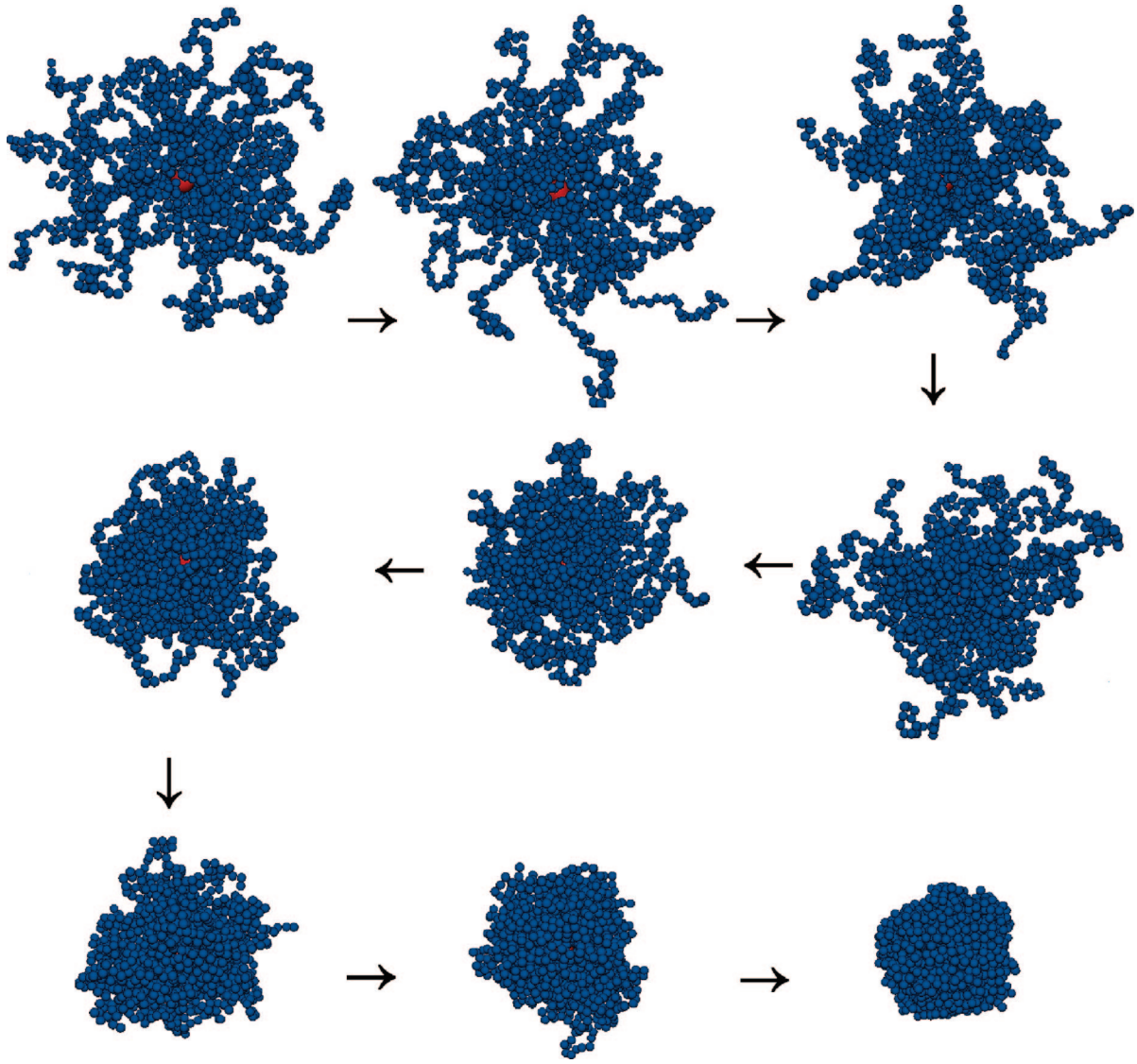

Figure 2. Simulation snapshots of stars with functionality $f = 30$ to illustrate the coil-to-globule transition going from the athermal solvent to the poor solvent. The values of λ (following the arrows) are: top: $0 \rightarrow 0.10 \rightarrow 0.20$; middle: $0.30 \rightarrow 0.35 \rightarrow 0.41$; bottom: $0.50 \rightarrow 0.60 \rightarrow 1.00$.

the stars are swollen by virtue of the repulsive forces between the monomers. Upon increasing the parameter λ, the solvent-induced effective attraction between the monomers leads to a shrinking of the star. In the intermediate range of λ values, corresponding to solvents in the vicinity of the Θ point, the star is no longer fully swollen, nor is it compact, as can be seen from the snapshots. If λ is increased even further, then one enters the poor solvent regime, and the star collapses to a compact globule. The dependence of the gyration radius, R_G, on λ is shown in Figure 3a, which displays a steady decay as λ grows, featuring inflection points in the vicinity of $\lambda = 0.4$.

To estimate the Θ point of the stars, we take advantage of the scaling predictions of the blob model of Daoud and Cotton.[17] According to it, the star size, characterized by the radius of gyration, R_G, scales as $R_G \propto N^{3/5}f^{1/5}$ for athermal solvents and $R_G \propto N^{1/2}f^{1/4}$ for Θ solvents. The latter can be exploited, as is shown in Figure 3b, to obtain an estimation of the Θ point by plotting the scaled radius of gyration $R_G/(N^{1/2}f^{1/4})$ versus λ and determine the point of intersection of the curves corresponding to stars with different functionality. If the Daoud−Cotton scaling were fulfilled, then a single point of intersection would have been obtained; instead, we obtain a region in which all three curves run close to each other and which is centered at $\lambda_\Theta = 0.48$. We therefore take the latter value to be an estimate of the Θ point. The method employed here is similar to the one used for linear chains by Steinhauser;[55] the difference is that we use the functionality to increase the total number of monomers per molecule.

The Θ point is not a single defined quantity for all stars with a given monomer−monomer interaction, but rather it depends on the given values of f and N. This is not surprising because the connectivity of the arms of the star as well as their lengths result in different monomer concentrations in central and outer regions, which lead to variations in the value of λ corresponding to the Θ solvent. In this sense, it is more appropriate to speak about a Θ region for the stars. Only in the limit $N \rightarrow \infty$ do the Θ temperatures of stars and linear chains coincide, at which point they also become f-independent.[24]

B. Density Profiles. With the goal of examining the star polymer conformations, we consider the radial density profile, $\rho(r)$, to be a function of the distance, r, to the star center, obtained from simulations via eq 7. In Figure 4, we show the density profiles obtained from our simulations of a star with functionality $f = 30$ and for an athermal ($\lambda = 0$) and close to the Θ solvent ($\lambda = 0.41$). As expected, the monomers for the lower quality solvent are located closer to the center of the star; that is, the density profile shrinks, and it also appears to decay faster than that of the athermal star at the periphery.

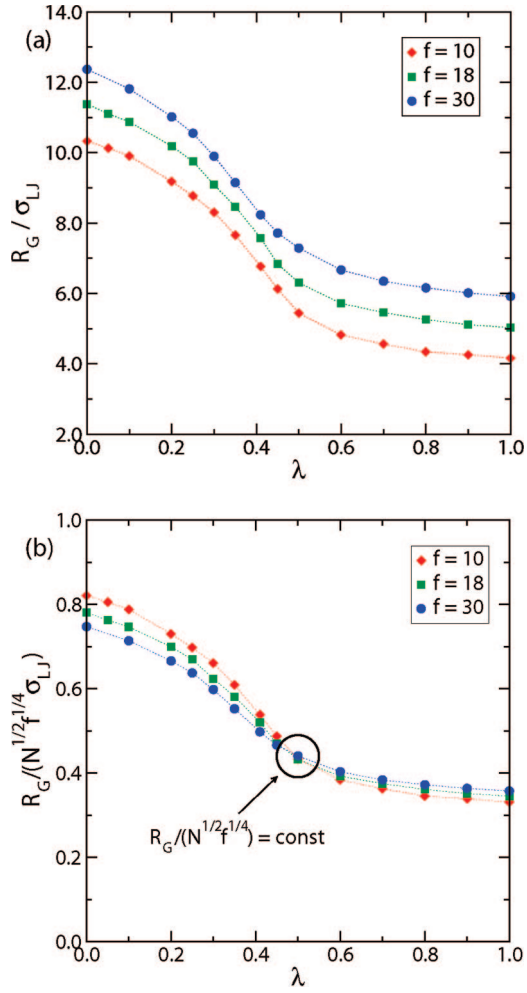

Figure 3. Simulation results for (a) the radius of gyration, R_G, as a function of the solvent quality. (b) The intersection of the scaled radius of gyration for different functionalities indicates that the coil-to-globule transition lies at $\lambda \cong 0.48$.

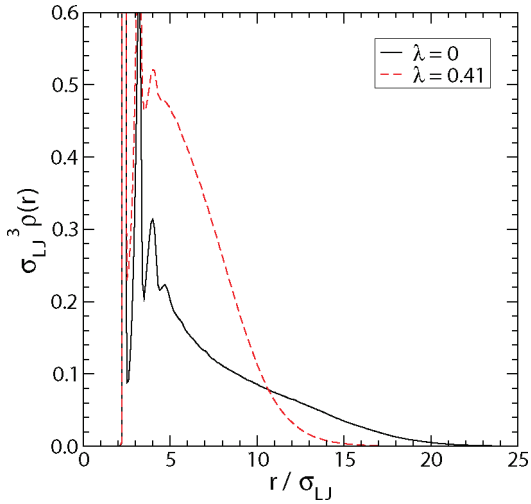

Figure 4. Simulation results for the density profile, $\rho(r)$, for a star with functionality $f = 30$ in athermal ($\lambda = 0$) and close to Θ solvent ($\lambda = 0.41$) plotted against the distance from the center, r, in units of the LJ diameter, σ_{LJ}.

A starting point for a quantitative description of the profiles is offered by the Daoud−Cotton blob model for athermal and Θ solvent for stars with sufficiently long arms. The blob model states that in the scaling regime in the interior of the star, the following power-law dependencies of $\rho(r)$ on r hold[17]

$$\rho_{ath}(r) \propto r^{-4/3} \tag{12}$$

$$\rho_{\Theta}(r) \propto r^{-1} \tag{13}$$

In the outer region of the star, the scaling behavior of the density profile is no longer valid. It can rather be described as a dilute polymer solution, for which the local density is proportional to the local osmotic pressure $\Pi(r) \propto \rho(r)$. The latter takes the form[27]

$$\Pi(r) \propto \left(\frac{1}{r^2} + 2\kappa^2\right)\frac{\zeta}{R_k} \exp^{-\kappa^2(r^2-R_k^2)} \tag{14}$$

In eq 14 above, R_k denotes the corona radius, which, for athermal stars, has been shown[23,27] to take the value $R_k = (2/3)R_G$. Furthermore, κ is the inverse decay length of the diffuse density profile that must be on the order R_G^{-1}. Indeed, for athermal stars, the value $\kappa R_G = 0.95$ has been obtained.[23,27] Finally, ζ is a dimensionless quantity for which an expression will be derived below.

Following the arguments of Jusufi et al.,[27] we can now combine the scaling relation, eq 12, which is valid for $r \le R_k$, with the proportionality relation, $\rho(r) \propto \Pi(r)$, and eq 14, both of which are valid for $r > R_k$, to obtain the following ansatz for the density profile of athermal stars

$$\rho_{ath}(r) \propto \begin{cases} r^{-4/3}R_k^{-5/3} & r \le R_k \\ \left(\frac{1}{r^2} + 2\kappa^2\right)\frac{\zeta}{R_k} \exp\{-\kappa^2(r^2 - R_k^2)\} & r > R_k \end{cases} \tag{15}$$

Now the quantity ζ can be determined by imposing the condition of continuity of $\rho_{ath}(r)$ at $r = R_k$, leading to the value

$$\zeta = \frac{1}{1 + 2\kappa^2 R_k^2} \tag{16}$$

The validity of the density modeling of eq 15 was confirmed by Mayer and Likos,[23] who compared MD simulation results for athermal stars with different functionalities and degrees of polymerization.

Following the same argumentation, we set forward the hypothesis that by combining eq 13 with eq 14 the density profile of Θ-like stars can also be modeled as

$$\rho_{\Theta}(r) \propto \begin{cases} r^{-1}R_k^{-2} & r \le R_k \\ \left(\frac{1}{r^2} + 2\kappa^2\right)\frac{\zeta}{R_k} \exp\{-\kappa^2(r^2 - R_k^2)\} & r > R_k \end{cases} \tag{17}$$

Although the expressions for $\rho_{ath}(r)$ and $\rho_{\Theta}(r)$ are given by different power laws in the region $r \le R_k$, the parameter ζ is given by the same expression, eq 16 for both, because it evidently guarantees the fulfillment of continuity of the profile. However, there is no reason to expect that the values of the dimensionless parameters κR_G and R_k/R_G will be the same for athermal and thermal stars. In fact, because Θ-like stars are more compact than athermal stars, it is to be expected that R_k will lie closer to R_G and that the decay length in the diffuse region will be smaller, thus leading to a higher value of κR_G than that for athermal stars. These expectations will be shortly confirmed.

In the spirit of the coarse-graining approach and the scaling behavior of polymeric systems, one can attempt to introduce suitable dimensionless variables, scaling, for example, all quantities with dimensions of length with the gyration radius R_G, with the goal of collapsing the density profiles of stars with different functionalities, f, and polymerizations per arm, N, onto

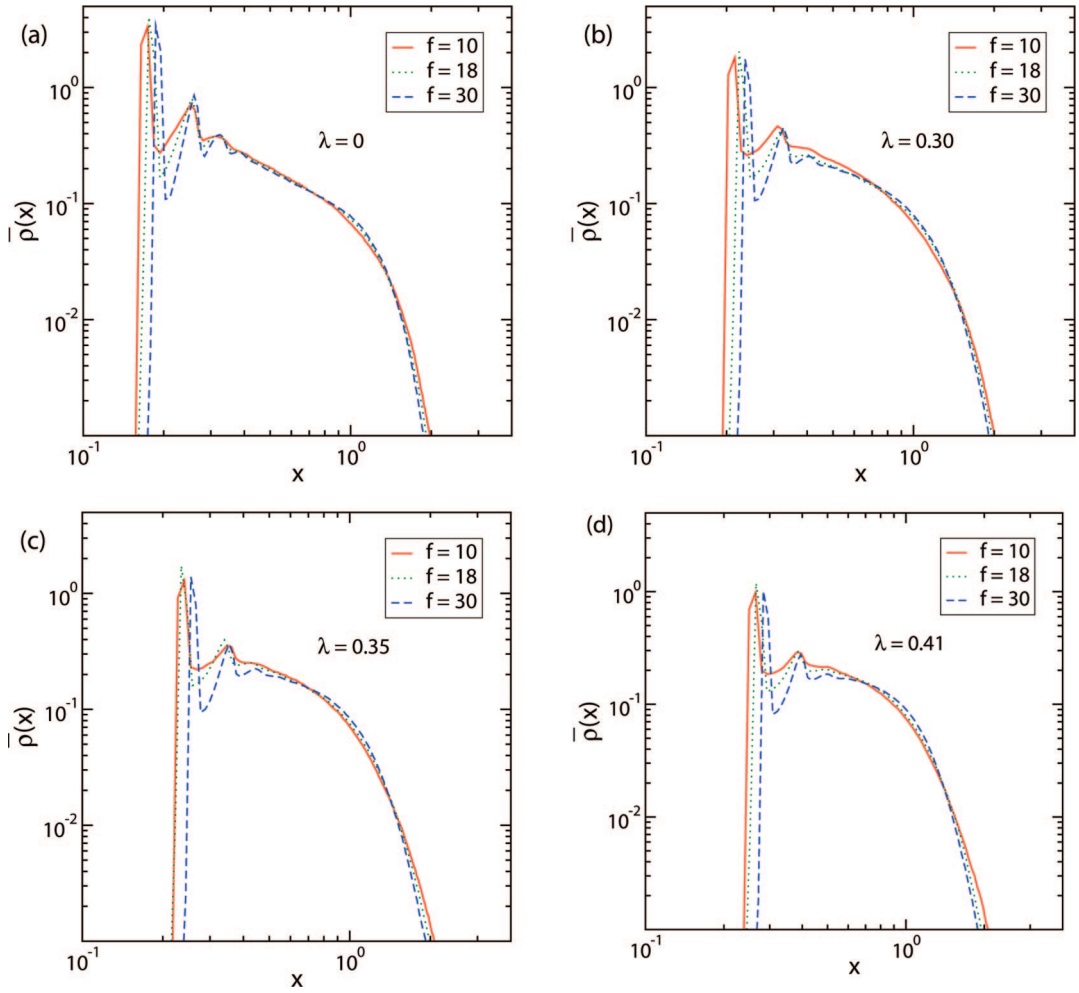

Figure 5. Scaled density profiles $\bar{\rho}(x)$ obtained via eq 19 for stars under different solvent conditions.

universal, master curves. Indeed, the modeling of eqs 15 and 17 above is already suggesting such a possibility, provided that the parameters κR_G and R_k/R_G are f- and N-independent for given solvent quality. To test this possibility, we first use the radius of gyration as the typical length scale. Furthermore, because the total number of monomers is given by the product of the functionality, f, and the degree of polymerization, N, the profiles must fulfill the normalization condition

$$\int_0^\infty \mathrm{d}^3 r \rho(r) = Nf \tag{18}$$

We thus introduce a normalized density, $\bar{\rho}(x)$, to be

$$\bar{\rho}(x) \equiv \frac{R_G^3}{Nf}\rho(r) \tag{19}$$

where $x \equiv r/R_G$ is the dimensionless distance from the star center. In principle, modeling of the profiles by means of eqs 15 and 17 is possible and useful if the density profiles, $\rho(r)$, for different stars collapse onto one another of scaled according to eq 19 above.

To demonstrate the universal behavior of the radial density profiles, we scale the MD results with the factor $R_G^3/(Nf)$ from eq 19 and plot $\bar{\rho}(x)$ versus x for stars with functionality $f = 10$, 18, and 30 and for various solvent qualities in Figure 5. For small distances, x, from the star center, a shell-like structure of the monomers around the core region is observed. The variable size of the core as function of the functionality leads to small shifts in the oscillations of the density in the vicinity of the center. For sufficiently long arms, however this simulation artifact can be disregarded, and we find a region between $R_G/3$ and R_G from the star center, where the scaling behavior is observed. This region becomes smaller for lower solvent qualities. For larger distances, we see the exponential decay of the density profiles. Most importantly, we find the collapse of the density profiles for different stars to be valid for all solvent qualities in the range from athermal solvents to those lying close to the Θ region.

The collapse of the density profiles, $\bar{\rho}(x)$, for various functionalities confirms the existence of a universal curve that for Θ-like solvents can now easily be derived from eq 17. Here we introduce the dimensionless quantities $\bar{R}_k \equiv R_k/R_G$ and $\bar{\kappa} \equiv \kappa R_G$ and obtain

$$\bar{\rho}(x) = A(\bar{\kappa})\begin{cases} x^{-1}\bar{R}_k^{-2} & x \le \bar{R}_k \\ \left(\dfrac{1}{x^2} + 2\bar{\kappa}^2\right)\dfrac{\zeta}{\bar{R}_k}\exp\{-\bar{\kappa}^2(x^2 - \bar{R}_k^2)\} & x > \bar{R}_k \end{cases} \tag{20}$$

where $A(\bar{\kappa})$ is a normalization factor that follows from the constraint $\int \mathrm{d}^3 x \bar{\rho}(x) = 1$ and is given by

$$A(\bar{\kappa}) = \left[2\pi + 4\pi\zeta\left(1 + \frac{\sqrt{\pi}}{\bar{\kappa}\bar{R}_k}\exp\{\bar{\kappa}^2\bar{R}_k^2\}\,\mathrm{Erfc}\{\bar{\kappa}\bar{R}_k\}\right)\right]^{-1} \tag{21}$$

where $\mathrm{Erfc}(z)$ is the complementary error function.

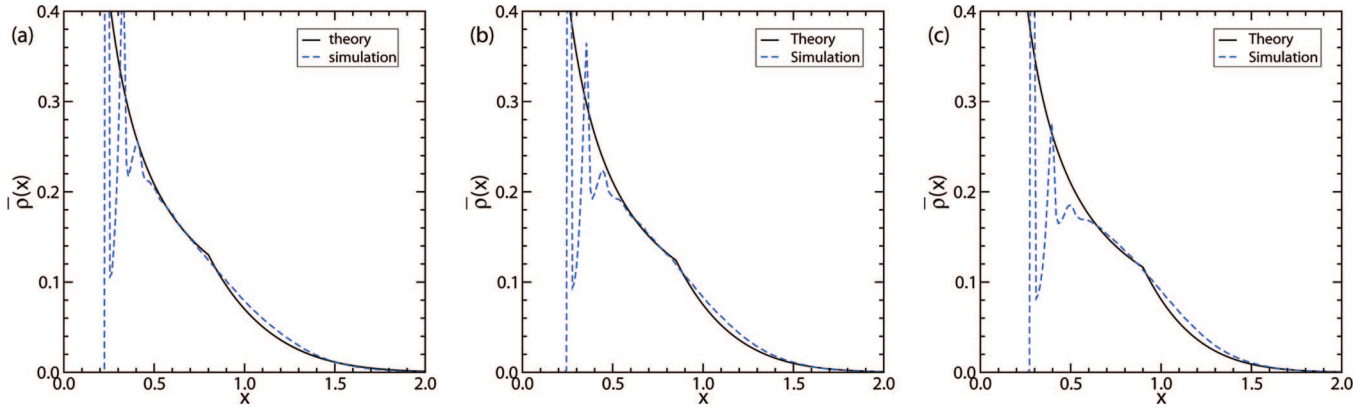

Figure 6. Scaled density profile $\bar{\rho}(x)$ for a $f = 30$ star from simulation and from theory, according to eqs 20 and 21 at (a) $\lambda = 0.30$, (b) $\lambda = 0.35$, and (c) $\lambda = 0.41$.

In Figure 6a, we show the simulation result for the quantity $\bar{\rho}(x)$ for a star with $f = 30$ and $N = 50$ at solvent quality $\lambda = 0.30$, together with the fit by eqs 20 and 21. It can be seen that although it is derived strictly for the Θ solvent, the universal expression 20 also produces good results for intermediate solvent qualities. As anticipated, the values of the parameters $\bar{\kappa}$ and $\bar{R}_k$ are different and, in fact, higher than those for the athermal solvents: the fit for $\lambda = 0.30$, Figure 6a, was obtained with $\bar{\kappa} = 1.15$ and $\bar{R}_k = 0.8$, cf. $\bar{\kappa} = 0.95$ and $\bar{R}_k = 0.667$ for athermal solvents. The cases $\lambda = 0.35$ and 0.41 are shown in Figure 6b, with parameter values $\bar{\kappa} = 1.22$ and $\bar{R}_k = 0.85$, and Figure 6c, where $\bar{\kappa} = 1.28$ and $\bar{R}_k = 0.9$. Indeed, the values depend on solvent quality and grow with λ, as anticipated. Figure 7 shows the original density profiles, $\rho(r)$, for various λ values in a double-logarithmic representation. Here for $\lambda = 0$, the scaling behavior of eq 12 can be seen; the situation close to the Θ solvent, $\lambda = 0.41$, for which a $\rho(r) \propto r^{-1}$ behavior, where eq 13 should be satisfied, is less clear because the power law does not extend to a sufficiently broad region in r because the individual chains are not long enough; similar results were found by Grest.[26] However, it is evident that the athermal solvent behavior, $\rho(r) \propto r^{-4/3}$ is already lost for solvents of intermediate quality, $\lambda = 0.30$. In this sense, the case $\lambda = 0.30$ can be characterized as lying in between the athermal and Θ limits, a fact that will also manifest itself in the results for the effective force, shown in the section that follows.

IV. Effective Interaction

We measured the effective force between stars in the simulation by applying the procedure described in Section II, and, in particular, by calculating the averages over the microscopic forces, eq 8. In Figure 8, we show simulation snapshots of two pairs of interacting star polymers at close separations for both athermal solvents ($\lambda = 0$, left panel) and close-to-Θ solvents ($\lambda = 0.41$, right panel). From simple inspection, it can be anticipated that the forces exerted on the central particles will be very different in the two cases because these are mediated by the surrounding chains, and the latter have vastly different configurations in the two cases. As it has been pointed out elsewhere,[21] when comparing with theoretical models in which the size of the central core on which the chains are grafted is ignored, one has to correct for the presence of a small central core in the simulation. In particular, the presence of the finite core of radius, R_c, of both star polymers leads to a divergent force at a distance $2R_d = 2R_c + \sigma_{LJ}$. Accordingly, the value $2R_d$ will be subtracted from the center-to-center distance D for all simulation results that follow so that the force will diverge at $D - 2R_d = 0$; the forces expressed on this "shifted separation" will then be compared with theoretical values.

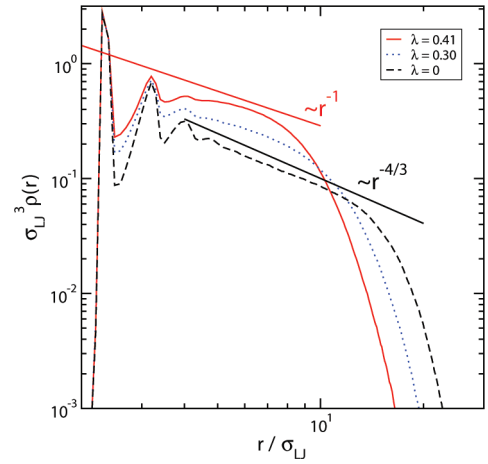

Figure 7. Scaling behavior for three different values of λ for a star with functionality $f = 30$.

We begin with the known case of athermal solvents to confirm established results for this situation.[2,21] The results for the measured effective forces between two athermal stars are shown in Figure 9a, together with the theoretical prediction,[2] $F(D) = -\mathrm{d}V_0(D)/\mathrm{d}D$ on the basis of the logarithmic Yukawa effective potential, $V_0(D)$

$$v_0(D) = \frac{5}{18} f^{3/2} \begin{cases} -\ln\left(\frac{D}{\sigma_k}\right) + \frac{1}{1+\sqrt{f}/2}; & D \le \sigma_k \\ \frac{1}{1+\sqrt{f}/2}\left(\frac{\sigma_k}{D}\right) \exp\left(-\frac{\sqrt{f}(D-\sigma_k)}{2\sigma_k}\right); & D > \sigma_k \end{cases} \tag{22}$$

In eq 22 above, $\sigma_k \equiv 2R_k$ is the corona diameter and is thus related to the gyration radius, R_G, via $\sigma_k = (4/3)R_G$, as found in the simulations of Jusufi et al.[21] The kinks in the force versus distance theoretical curves in Figure 9a, visible at $D = \sigma_k$, arise from the fact that $V_0(D)$ is continuous only up to its first derivative with respect to D there, a fact that has no further consequences, however. The constant value of the ratio σ_k/R_G for athermal stars, in conjunction with eq 22 above, implies that the quantity $FR_G/(f^{3/2}k_BT)$ should be a universal function of D/R_G for $D/\sigma_k \le 1$ for all f values, and it should feature a weak dependence on $f^{1/2}$ at larger separations because of the prefactor, $1/(1 + f^{1/2}/2)$, and the decay length proportional to $1/f^{1/2}$ in the exponent. The inset of Figure 9a confirms this fact. Evidently, a purely repulsive interaction between athermal stars is obtained, with the corresponding effective potential diverging

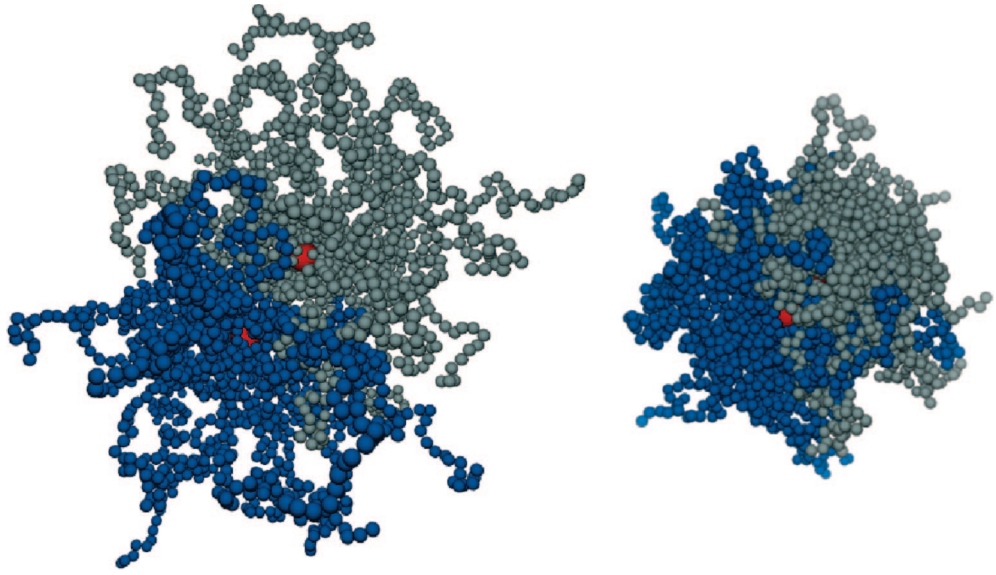

Figure 8. Simulation snapshots of two interacting stars with functionality $f = 30$ in an athermal solvent (left panel) and close-to-Θ solvent (right panel).

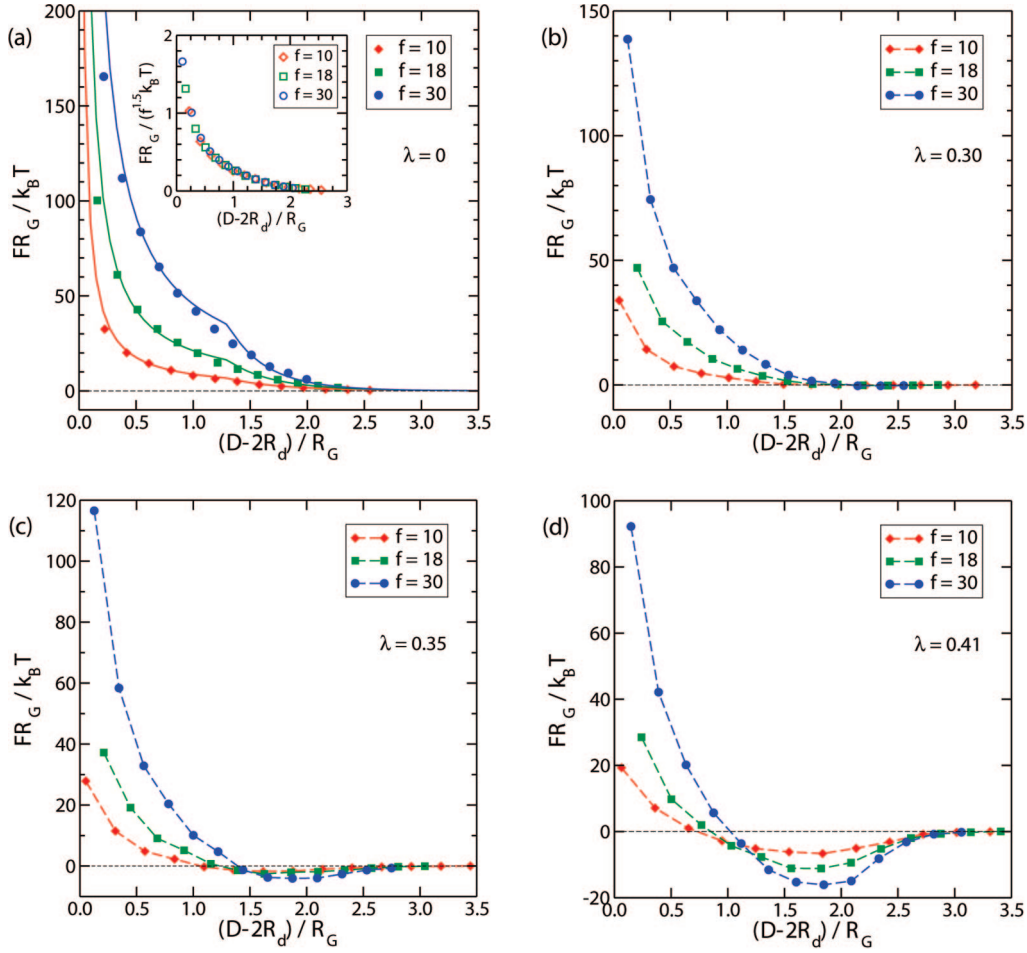

Figure 9. Effective force plotted against the reduced distance, $D - 2R_d$, between two stars under different solvent conditions: (a) athermal solvents ($\lambda = 0$), (b) $\lambda = 0.30$, (c) $\lambda = 0.35$, and (d) $\lambda = 0.41$. The solid lines in panel a are the theoretical curves, and the inset illustrates that the data collapse when scaled appropriately.

logarithmically for separations smaller than the corona diameter, σ_k, and with a Yukawa-like decay otherwise. The results confirm earlier findings by Jusufi et al.[21] as well as by von Ferber et al.[57]

Next we consider the case $\lambda = 0.30$. As seen in Figure 9b, the effective star−star force remains purely repulsive; the monomer−monomer attractions, which are quite pronounced in this case (Figure 1), are not yet sufficiently strong to bring about net star attractions. Evidently, this is also the case for all values of $\lambda \leq 0.3$. At the same time, a very significant reduction of both the strength and the range of the repulsive forces results. Note that distances in Figure 9 are scaled with the gyration

radius, R_G, under the corresponding solvent conditions so that a reduction of solvent quality has a double effect on the correlations of a concentrated solution of stars with a given number density, ρ. First, the physically relevant, dimensionless density ρR_G^3 decreases by a factor α^3, where $\alpha < 1$ is the ratio of the gyration radius of the star at the given solvent quality to that under athermal conditions. Second, the effective interaction itself reduces both its range and, most importantly, its repulsive strength. In this sense, the results found here can offer ample explanation of the effects of thermally reversible gelation experimentally found for stars.[34,35] The theoretical approach of Rissanou et al.[40−42] was based on an effective potential that does not change its shape with temperature[36] so that only the first of the above effects was taken into consideration. The second one further adds to the propensity of an arrested system to flow as the temperature is lowered. In addition, our findings corroborate the earlier, phenomenological approach to the effective interaction between stars in solvents of intermediate quality (but still above the Θ temperature) for which purely repulsive effective interactions were employed to describe theoretical SANS data.[36]

Some weak attractions between thermal stars appear for the case $\lambda = 0.35$, bringing us closer to the Θ region at $\lambda_\Theta \cong 0.48$. (See Figure 9c.) The threshold for the appearance of attractive forces therefore lies between $\lambda = 0.30$ and 0.35, but it seems to be closer to the former than to the latter. The attractions are nevertheless weak, and they will barely have any effect on the structural correlations or the thermodynamics; a concentrated star−polymer system under such conditions will maintain stability against a phase separation into a dilute and a dense phase (liquid/gas coexistence). The appearance of effective attractive forces above the Θ point is also in agreement with the findings of Krakoviack et al.[58] on polymer chains, for which the center-of-mass representation was employed. In regard to the quantitative features of the attractive part of the force, we see from Figure 9c that for a given solvent quality, its range is reduced but its strength is enhanced as f grows. The overall contribution of the attractive forces certainly grows with f because of the increased number of mutually attracting monomers. At the same time, the steric repulsions between the arms also become stronger with f, albeit with a different power of f than the attractive ones and with a different D dependence. This competition brings about the features mentioned above regarding the range and strength of the forces, as will be confirmed by a perturbative theoretical description of the effective interactions below. Finally, for even lower solvent quality, that is, $\lambda = 0.41$ (Figure 9d), very pronounced attractions have developed whose range and depth characteristics follow the same trends as those found for the $\lambda = 0.35$ case.

In an attempt to describe the effective star forces in thermal solvents theoretically and to obtain insight into the mechanisms of competition between attractions and repulsions, we take advantage of the fact that the effective interaction between athermal stars, $V_0(D)$, is known[2] and given by eq 22. In view of the fact that the effective interaction remains repulsive or, at worst, it develops only very weak attractions also for solvents far from athermal ($\lambda = 0.35$), it is appealing to set up a perturbative approach in which the effects of the attractions between the monomers are superimposed to the steric repulsion in a mean-field fashion. In particular, we are proposing to split the effective interaction $V(D)$ between thermal polymers as

$$V(D) = V_0(D) + \Phi_{att}(D) \tag{23}$$

The origin of the effective attractive interaction $\Phi_{att}(D)$ arises purely from the term $v_{att}(r)$ in the monomer−monomer interaction for the thermal case (eq 10); the effects of $v_0(r)$ are incorporated on its coarse-grained counterpart, the effective potential $V_0(D)$. For $\Phi_{att}(D)$, we employ a simple approximation of considering the overlap integral of the density profiles of the two unperturbed stars; that is, if we employ the density profile from eq 17, then we can express the attractive part of the star−star interaction potential at a relative distance, D, as an overlap integral over all positions of the monomers

$$\Phi_{att}(D) = \int\int d^3r d^3r' \rho(|\mathbf{r}|)\rho(|\mathbf{D} - \mathbf{r}'|) v_{att}(|\mathbf{r} - \mathbf{r}'|) H(|\mathbf{r} - \mathbf{r}'| - r_{cut}) \tag{24}$$

with $H(r)$ being the Heaviside step function.

Before proceeding to the results, a few remarks must be made regarding the approximations inherent in writing down eq 24 above. First, and contrary to the usual perturbation approaches in the realm of simple fluids in which the correlation functions of the reference system are used in the perturbation term, here we employ the density profiles of the stars corresponding to the λ value under consideration. These are readily available from the simulation of isolated stars and modeled by eq 17. Second, we have made the crude approximation of modeling the two-body monomer density as a product of the two unperturbed density profiles, which is not very realistic in view of the fact that arms from the two different stars will retract and the stars will deform. Because the monomer−monomer attractive interaction, $v_{mm}(r)$, is long-range and decaying as a power law, this may not be crucial as far as interactions between distant monomers are concerned; however, short-range correlations, and the exclusion of each bead from the immediate neighborhood of another one, arising from the steric interactions $v_0(r)$ must be taken into account to avoid an overestimation of the attractive contributions. We model these by the Heaviside step function, $H(r)$, in eq 24 above by introducing a short-range cutoff, r_{cut}, below which the beads cannot approach. Evidently, r_{cut} must be on a microscopic scale; we used r_{cut} as a fit parameter and indeed microscopic values that had a very weak dependency on f and λ. Finally, we iterate that the approximation above is perturbative in its spirit, utilizing λ (which is an overall factor in the integration kernel, $v_{att}(r)$) as a coupling constant. Therefore, its success depends on the degree of deviation of the profiles, $\rho(r)$, from the athermal ones, which give rise to the reference effective interaction, $V_0(D)$.

Fits of the density profiles (eq 20 and Figure 6) provide us with the needed values of $\bar{\kappa}$ and $\bar{R}_k$, which are presented in Section III.B. Accordingly, only r_{cut} is required to perform the calculation of the attractive effective interaction potential. Afterward, the theoretical prediction for the effective force, $F(D) = -dV(D)/dD$ can be compared with the simulation results. The best fit to our simulation data is obtained by choosing $r_{cut} = 2.8\sigma_{LJ}$ for an $f = 10$ star, whereas the stars with functionalities of 18 and 30 lead to values that were approximately 5−10% higher.

The results from this theoretical approach compared with the MD effective forces are shown in Figure 10. Figure 10a shows the competition between the effective repulsion, $V_0(D)$, and the mean-field attractive term. For solvents of even marginal quality, $\lambda = 0.35$, we find good agreement between the theoretical approach and the simulation, at least for separations that are not too small; note, however, that for star polymer solutions close to their overlap concentration (and also considerably higher ones), for which the interesting phenomena of reversible vitrification take place,[34,35] the precise values of the effective interaction at short separations are irrelevant as long as they are much higher than k_BT, as is indeed the case here. The success of the theory is not completely surprising because the real density profiles of the stars have been used, albeit in the simple overlap approximation. Note that the kink in the theoretical forces is inherited from the form of $V_0(D)$, as discussed before.

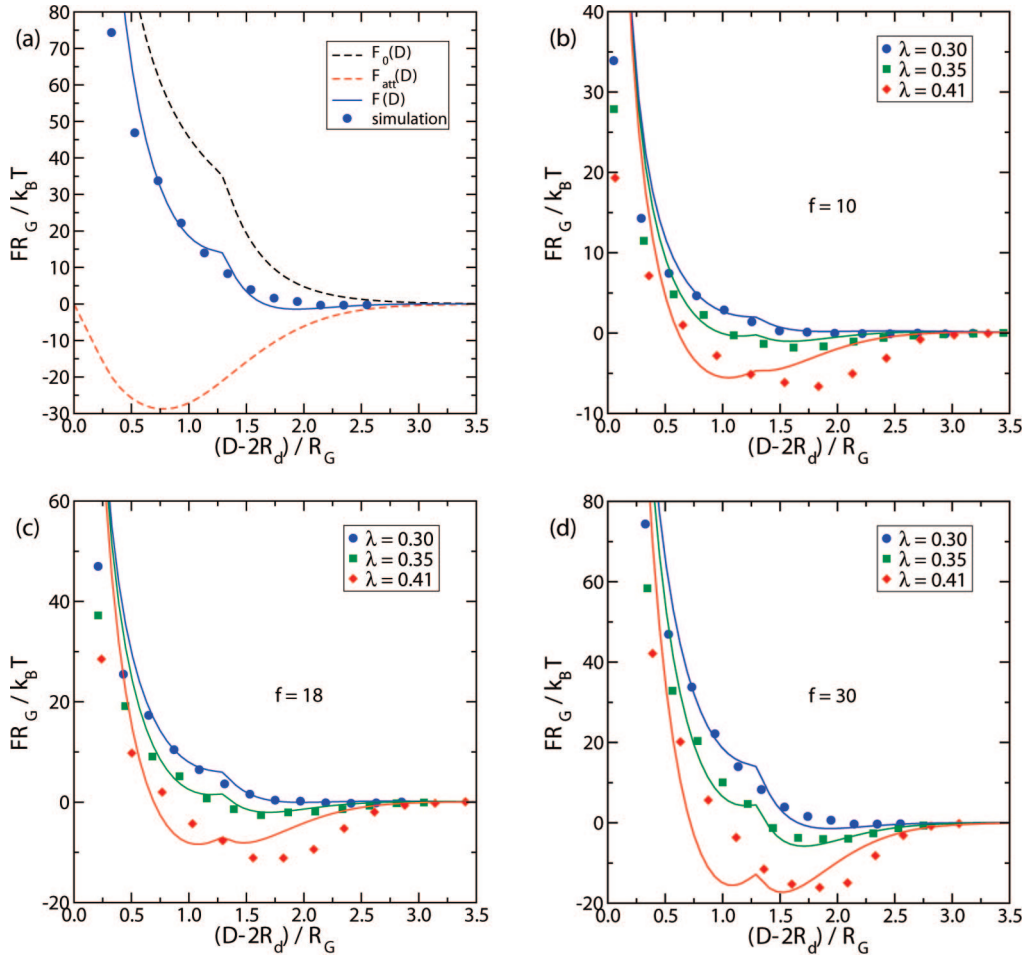

Figure 10. (a) Reference (repulsive, $F_0(D)$) and perturbation (attractive, $F_{att}(D)$) contributions to the total effective force, $F(D)$, between two thermal stars for a functionality, $f = 30$, in solvent with $\lambda = 0.30$, together with the simulation result. Results for the different solvents are shown for stars with functionalities: (b) $f = 10$, (c) $f = 18$, and (d) $f = 30$. The points denote results from the simulation and the lines denote results from the perturbative approach described in the text.

The perturbative nature of the theory causes it to break down for $\lambda = 0.41$, as can be seen in Figure 10b−d. This is associated with an overestimation of the attraction between stars at short distances, which cannot be corrected via the cutoff range, r_{cut}; here, the steric term $V_0(D)$ is not valid as a reference anymore because the profiles are drastically different from their athermal counterparts, which are responsible for the form of $V_0(D)$. Nevertheless, the success of the theory in making realistic predictions for solvent qualities markedly different from athermal ones, that is, up to $\lambda = 0.35$, offers the possibility to calculate or make a quantitative estimate of $V(D)$ without having to resort to expensive simulations involving two star polymers. Indeed, all that is needed is the profile $\rho(r)$ of an isolated star, and this can be obtained by either a much cheaper single-star simulation, or it can be readily modeled by eq 20.

V. Summary and Conclusions

We have performed MD simulations for star polymers with different functionalities and in solvents of various quality, ranging from the athermal solvent to poor solvents. The main focus was placed on solvents of intermediate quality, particularly as the Θ point is approached. The latter has been estimated by making use of the Daoud−Cotton model, which predicts the scaling behavior of the gyration radius for f and N. We have demonstrated that the monomer density profiles for star polymers, even in thermal solvents, can be collapsed on master curves (a different curve for each solvent quality) when appropriate scaled variables are used. In this way, any explicit reference to N and f can be scaled out, and the two quantities appear implicitly only in the way that they influence the overall size, R_G, of the star and in the form of a trivial normalization constant. This allows a mesoscopic modeling of the density profiles of stars in which their overall size appears to be the only length scale.

We have further calculated the center-to-center effective forces between stars, showing that they remain repulsive for a broad range of intermediate solvent qualities and start developing attractions for marginal solvents. The simulations have been complemented by a mean-field approach for the effective interactions, which works quite well up to the point in which significant effective attractions appear. It would be desirable to improve on this theory, for example, by a more accurate modeling of the distorted monomer profiles as the two stars closely approach each other, so as to be able to deal with solvents that are very close, or even slightly below, the Θ condition. Yet, this work goes quite some way in filling a long-standing gap because an approach that is capable of extending the effective star−star interactions from the well-studied athermal case to the marginally good ones was hitherto lacking. Future work should focus on exploring the many-body correlations, the thermodynamics, and the thermally induced rheology modifications of concentrated star solutions by employing the coarse-grained approach put forward in this article. The bridging of the length scales achieved by the derivation of an effective interaction is the crucial step that has been missing in the effort of pursuing such investigations, and it should have implications

on other thermally sensitive soft colloids, such as microgels or core−shell block-copolymer micelles.

Acknowledgment. Useful exchanges with Prof. Dimitris Vlassopoulos and Dr. Anastasia Rissanou (both in FO.R.T.H., Heraklion, Greece) are gratefully acknowledged. We thank the Erwin Schrödinger International Institute for Mathematical Physics (ESI, Vienna), where parts of this work were carried out, for its hospitality.

References and Notes

(1) Grest, G. S.; Fetters, L. J.; Huang, J. S.; Richter, D. *Adv. Chem. Phys.* **1996**, *94*, 67.
(2) Likos, C. N.; Löwen, H.; Watzlawek, M.; Abbas, B.; Jucknischke, O.; Allgaier, J.; Richter, D. *Phys. Rev. Lett.* **1998**, *80*, 4450–4453.
(3) Watzlawek, M.; Likos, C. N.; Löwen, H. *Phys. Rev. Lett.* **1999**, *82*, 5289.
(4) Bang, J.; Lodge, T. P.; Wang, X.; Brinker, K. L.; Burghardt, W. R. *Phys. Rev. Lett.* **2002**, *89*, 215505.
(5) Lodge, T. P.; Bang, J.; Park, M. J.; Char, K. *Phys. Rev. Lett.* **2004**, *92*, 145501.
(6) Vlassopoulos, D.; Fytas, G.; Pakula, T.; Roovers, J. *J. Phys.: Condens. Matter* **2001**, *13*, R855–R876.
(7) Vlassopoulos, D. *J. Polym. Sci., Part B: Polym. Phys.* **2004**, *42*, 2931–2941.
(8) Foffi, G.; Sciortino, F.; Tartaglia, P.; Zaccarelli, E.; Verso, F. L.; Reatto, L.; Dawson, K. A.; Likos, C. N. *Phys. Rev. Lett.* **2003**, *90*, 238301.
(9) Stiakakis, E.; Vlassopoulos, D.; Likos, C. N.; Roovers, J.; Meier, G. *Phys. Rev. Lett.* **2002**, *89*, 208302.
(10) Zaccarelli, E.; Mayer, C.; Asteriadi, A.; Likos, C. N.; Sciortino, F.; Roovers, J.; Iatrou, H.; Hadjichristidis, N.; Tartaglia, P.; Löwen, H.; Vlassopoulos, D. *Phys. Rev. Lett.* **2005**, *95*, 268301.
(11) Mayer, C.; Zaccarelli, E.; Stiakakis, E.; Likos, C. N.; Sciortino, F.; Munam, A.; Gauthier, M.; Hadjichristidis, N.; Iatrou, H.; Tartaglia, P.; Löwen, H.; Vlassopoulos, D. *Nat. Mater.* **2008**, *7*, 780–784.
(12) Likos, C. N. *Phys. Rep.* **2001**, *348*, 261–439.
(13) Likos, C. N. *Soft Matter* **2006**, *2*, 478.
(14) Jusufi, A.; Likos, C. N.; Löwen, H. *Phys. Rev. Lett.* **2002**, *88*, 018301.
(15) Jusufi, A.; Likos, C. N.; Löwen, H. *J. Chem. Phys.* **2002**, *116*, 11011.
(16) Shusharina, N. P.; Rubinstein, M. *Macromolecules* **2008**, *41*, 203.
(17) Daoud, M.; Cotton, J. P. *J. Phys. (Paris)* **1982**, *43*, 531–538.
(18) Grest, G. S.; Kremer, K.; Witten, T. A. *Macromolecules* **1987**, *20*, 1376–1383.
(19) Batoulis, J.; Kremer, K. *Macromolecules* **1989**, *22*, 4277.
(20) Yethiraj, A.; Hall, C. K. *J. Chem. Phys.* **1991**, *94*, 3943.
(21) Jusufi, A.; Watzlawek, M.; Löwen, H. *Macromolecules* **1999**, *32*, 4470–4473.
(22) Hsu, H.-P.; Nadler, W.; Grassberger, P. *Macromolecules* **2004**, *37*, 4658–4663.
(23) Mayer, C.; Likos, C. N. *Macromolecules* **2007**, *40*, 1196–1206.
(24) Batoulis, J.; Kremer, K. *Europhys. Lett.* **1988**, *7*, 683.
(25) Bishop, M.; Clarke, J. H. R. *J. Chem. Phys.* **1989**, *90*, 6647.
(26) Grest, G. S. *Macromolecules* **1994**, *27*, 3493–3500.
(27) Jusufi, A.; Dzubiella, J.; Likos, C. N.; von Ferber, C.; Löwen, H. *J. Phys.: Condens. Matter* **2001**, *13*, 6177–6194.
(28) Benzouine, F.; Benhamou, M.; Himmi, M. *Eur. Phys. J. E* **2004**, *13*, 345–351.
(29) Benhamou, M.; Himmi, M.; Benzouine, F.; Bettachy, A.; Derouiche, A. *Eur. Phys. J. E* **2004**, *13*, 353–358.
(30) Senff, H.; Richtering, W. *J. Chem. Phys.* **1999**, *111*, 1705.
(31) Lyon, L. A.; Debord, J. D.; Debord, S. B.; Jones, C. D.; McGrath, J. G.; Serpe, M. J. *J. Phys. Chem. B* **2004**, *108*, 19099.
(32) Wiedemair, J.; Serpe, M. J.; Kim, J.; Masson, J. F.; Lyon, L. A.; Mizaikoff, B.; Kranz, C. *Langmuir* **2007**, *23*, 130.
(33) Suzuki, D.; McGrath, J. G.; Kawaguchi, H.; Lyon, L. A. *J. Phys. Chem. B* **1999**, *111*, 5667.
(34) Kapnistos, M.; Vlassopoulos, D.; Fytas, G.; Mortensen, K.; Fleischer, G.; Roovers, J. *Phys. Rev. Lett.* **2000**, *85*, 4072.
(35) Stiakakis, E.; Vlassopoulos, D.; Loppinet, B.; Roovers, J.; Meier, G. *Phys. Rev. E* **2002**, *66*, 051804.
(36) Likos, C. N.; Löwen, H.; Poppe, A.; Willner, L.; Roovers, J.; Cubitt, B.; Richter, D. *Phys. Rev. E* **1998**, *58*, 6299.
(37) Millner, S. T.; Witten, T. A.; Cates, M. E. *Macromolecules* **1988**, *21*, 2610.
(38) Mewis, J.; Frith, W. J.; Strivens, T. A.; Russel, W. B *AIChE J.* **1989**, *35*, 415.
(39) Genz, U.; D'Aguanno, B.; Mewis, J.; Klein, R. *Langmuir* **1994**, *10*, 2206.
(40) Rissanou, A. N.; Vlassopoulos, D.; Bitsanis, I. A. *Phys. Rev. E* **2005**, *71*, 011402.
(41) Rissanou, A. N.; Yiannourakou, M.; Economou, I. G. *J. Chem. Phys.* **2006**, *124*, 044905.
(42) Rissanou, A. N.; Yiannourakou, M.; Bitsanis, I. A.; Economou, I. G. *Rheol. Acta* **2007**, *46*, 755–764.
(43) Glynos, E.; Chremos, A.; Petekidis, G.; Camp, P.; Koutsos, V. *Macromolecules* **2007**, *40*, 6947–6958.
(44) Sciortino, F.; Tartaglia, P.; Zaccarelli, E. *Phys. Rev. Lett.* **2003**, *91*, 268301.
(45) Cates, M. E.; Fuchs, M.; Kroy, K.; Poon, W.; Puertas, A. M. *J. Phys.: Condens. Matter* **2004**, *16*, S4861.
(46) Moreno, A. J.; Colmenero, J. *J. Chem. Phys.* **2006**, *125*, 016101.
(47) Moreno, A. J.; Colmenero, J. *J. Chem. Phys.* **2006**, *125*, 164507.
(48) Moreno, A. J.; Colmenero, J. *Phys. Rev. E* **2006**, *74*, 021409.
(49) Zaccarelli, E.; Saika-Voivod, I.; Moreno, A. J.; Buldyrev, S. V.; Tartaglia, P.; Sciortino, F. *J. Chem. Phys.* **2006**, *124*, 124908.
(50) Weeks, J.; Chandler, D.; Andersen, H. *J. Chem. Phys.* **1971**, *54*, 5237.
(51) Frenkel, D.; Smit, B. *Understanding Molecular Simulation: From Algorithms to Applications*; Academic Press: San Diego, 1996.
(52) Berendsen, H.; Postma, J.; van Gunsteren, W.; DiNola, A.; Haak, J. *J. Chem. Phys.* **1984**, *81*, 3684–3690.
(53) Doi, M. *Introduction to Polymer Physics*; Clarendon Press: Oxford, 1996.
(54) Murat, M.; Grest, G. S. *Macromolecules* **1996**, *29*, 1278–1285.
(55) Steinhauser, M. O. *J. Chem. Phys.* **2005**, *122*, 094901.
(56) Hansen, J. P.; MacDonald, I. R. *Theory of Simple Liquids*, 3rd ed.; Elsevier Academic Press: London, 2006.
(57) von Ferber, C.; Jusufi, A.; Watzlawek, M.; Likos, C. N.; Löwen, H. *Phys. Rev. E* **2000**, *62*, 6949–6956.
(58) Krakoviack, V.; Hansen, J.-P.; Louis, A. A. *Phys. Rev. E* **2003**, *67*, 041801.

MA8023359